EurJIC
European Journal of Inorganic Chemistry

Full Papers
doi.org/10.1002/ejic.202001134

Chemistry Europe
European Chemical Societies Publishing

Understanding the Incorporation and Release of Salicylic Acid in Metal-Organic Frameworks for Topical Administration

Sara Rojas[a] and Patricia Horcajada*[a]

Although metal-organic frameworks (MOFs) have been widely demonstrated to be great candidates for drug delivery applications, they have been mainly proposed for the intravenous route. Here, eight highly porous benchmarked MOFs, with different topologies and structures, are proposed for the topical delivery of salicylic acid (SA), an important, but highly reactive and unstable, therapeutically active metabolite of aspirin. The microporous Zr aminoterephthalate UiO-66-NH_2 was selected as the most promising SA carrier, achieving important loadings (12.1 wt.%). Finally, the SA delivery process was studied under simulated cutaneous conditions (aqueous media at 37 °C), reaching a plateau in 6 h (with ~64% or ~105.6 mg of released SA *per* g of UiO-66-NH_2). These results demonstrate the suitability of UiO-66-NH_2 for the topical controlled release of SA, making this formulation a promising candidate for the development of new devices for skin treatment.

Introduction

During the last decades, the development of controlled drug delivery systems (DDS) for the treatment of human diseases is growing very rapidly. DDS are designed to get a specific transport and progressively release of active pharmaceutical ingredients (APIs) for a long timeframe, protecting them from potential biodegradation and modifying their physicochemical properties (*e.g.*, solubility). Polymer-based drugs and DDS emerged from the laboratory bench in the 1900s as a promising therapeutic strategy for the treatment of certain devastating illnesses.[1] Among them, metal-organic frameworks (MOFs) are considered as great candidates for drug delivery applications, not only providing progressive release of the APIs but also modifying their biodistribution.[2–4] These hybrid materials, comprised of inorganic nodes and organic polycomplexant linkers that assemble into multidimensional periodic lattices through coordination bonds,[5] present several advantages as DDS: *i)* exceptional porosity associated with high drug cargoes; *ii)* highly versatile structures and compositions, potentially tunable depending on target API/site; *iii)* appropriate biological compatibility, stability and particle size; and *iv)* amphiphilic internal microenvironment, adapted to a large number of APIs, among others.[6] MOFs accomplished remarkable loadings (often much higher that traditional carrier systems) of a large variety of active molecules (drugs,[3,7,8] cosmetics,[9] biological gases),[10–12] with controlled releases under physiological conditions.

MOF-based DDS have been mainly proposed for the intravenous administration route, remaining other routes less studied Particularly, the skin, the largest organ in the body, is an attractive route for the delivery of therapeutics and represents a proven and smart option for treating a variety of cutaneous diseases (*e.g.*, acne, lymphoma, leishmaniosis). For instance, the topical drug delivery market is projected to reach 110 billion euros by 2025 (from 80 billion euros in 2020), at a compound annual growth rate (CAGR) of 6.4% during the forecast period.[13]

Although there have been many innovations in the development of new DDS, the number of effective topical cutaneous drugs remains small, primarily because of their instability within the formulation or skin, their uncontrolled release and the poor control of their skin permeation.[14]

Nonsteroidal anti-inflammatory drugs (NSAIDS) are a class of Cox-1 and/or Cox-2 inhibitors that suppress inflammation.[15] Particularly, the anti-inflammatory salicylic acid (SA), an important active metabolite of aspirin, has received significant attention because of its additional antibacterial, antifungal, and antipyretic activities. It has also shown promising results in the prevention of cardiovascular diseases and cancer.[16,17] Thus, an adapted release of SA may be desired for cutaneous antimicrobial and anti-inflammatory applications, such as treatment of infections or, even further, useful in biomedical devices as coatings. However, as a consequence of its highly reactive nature, its instability (half-life of 2–30 h)[18] is a major concern that needs to be addressed in order to use it as a potent topical drug.

Motivated by our prior studies on the use of MOFs for the cutaneous delivery,[9,19] and as impressive adsorbents of SA in gastrointestinal conditions,[20,21] here we propose the use of MOFs for the SA delivery. To reach a maximum SA cargo while

[a] *Dr. S. Rojas, Dr. P. Horcajada*
Advanced Porous Materials Unit (APMU)
IMDEA Energy Institute
Av. Ramón de la Sagra 3, 28935 Móstoles-Madrid, Spain
E-mail: patricia.horcajada@imdea.org

Supporting information for this article is available on the WWW under https://doi.org/10.1002/ejic.202001134

Part of the joint "Metals in Medicine" Special Collection with ChemMedChem.

understanding the adsorption process, we have rationally selected 8 highly porous benchmarked MOFs with different topologies and structures. First, a deep screening of the SA adsorption capacity of the MOFs and their stability was carried out, leading to the selection of the Zr aminoterephthalate UiO-66-NH_2. A deep study on the SA adsorption of UiO-66-NH_2 was performed using a large variety of techniques (powder X-ray diffraction-PXRD, thermogravimetric analysis-TGA, Fourier transform infrared-FTIR, N_2 sorption, elemental analysis-EA, high performance liquid chromatography-HPLC, etc.). Finally, the SA release from the loaded SA@UiO-66-NH_2 was evaluated under simulated cutaneous conditions.

Results and Discussion

Screening of the SA adsorption capacity and MOF stability

In order to obtain an efficient SA formulation for topical treatment, a high drug loading capacity rate was achieved through the selection of the best SA adsorbing material from a series of 8 MOFs. The selection of the MOF candidate for SA adsorption was based on the following criteria: *i)* exceptional porosity, compatible with the SA dimensions (7.5×6×2 Å^3; estimated by Vesta considering Van der Waal radii, Figure 1),[22] *ii)* their biocompatibility (*e.g.*, no sign of toxicity after the *in vivo* intravenous administration of very high doses of MIL-100;[23] after the oral administration of 1 g Kg^{-1} of MIL-127;[20] the exposure of zebrafish embryos with 200 μM of UiO-66 or MIL-100;[24] UiO-66, UiO-66-NH_2, MIL-53 or ZIF-8 against different cell lines),[25–27] or biosafety when using in humans cutaneous treatments,[19] and *iii) a priori* remarkable aqueous stability, which will avoid the possible toxicity of their degradation products (linkers and metals) during the drug delivery process. The series comprises: *1)* the microporous UiO-66 series based on zirconium(IV) oxoclusters and terephthalate anions (H_2BDC-X: 1,4-benzenedicarboxilic acid, where X = H, NH_2) **UiO-66** and **UiO-66-NH_2** ($[Zr_6O_4(OH)_4(C_8O_4H_3X)_6]\cdot nH_2O$);[28,29] *2)* the flexible porous **MIL-163** or $[Zr_2(C_{26}H_6O_6N_4)_2]\cdot(DMA)_5(H_2O)_{14}$; (DMA = *N*,*N*-dimethylamine) based on zirconium(IV) cations coordinated by 1,2,3-trioxobeneze groups;[30] *3)* the microporous **MIL-127** structure or $[Fe_3O(OH)_{0.88}Cl_{0.12}(C_{16}N_2O_8H_6)_{1.5}(H_2O)_3]\cdot nH_2O$ based on iron(III) octahedra trimers and 3,3′,5,5′-azobenzenetetracarboxylate anions;[31,32] *4)* the mesoporous **MIL-100** or $[Fe_3O(H_2O)OH(C_9H_6O_6)]\cdot nH_2O$ (H_3BTC: 1,3,5-benzenetricarboxylic acid or trimesic acid) based on iron(III) octahedra trimers and trimesate anions;[33] *5)* two flexible iron(III) terephthalates denoted as **MIL-53** and **MIL-53-(OH)$_2$** ($[Fe(OH)(C_8O_4H_2X_2)]$, where X = H and OH, respectively), which are 3D porous solids built up from chains of corner-sharing $[FeO_4(OH)_2]$ octahedra, connected through terephthalate linkers with potential structural adaptability for guest molecule diffusion;[34] and *6)* the microporous zeolitic imidazolate framework **ZIF-8** or $[Zn(C_4H_5N_2)_2]$, based on zinc(II) interconnected with 2-methylimidazole ligands (2-mIm) leading to a sodalite topology (see detailed porous properties in the Table 1).[35]

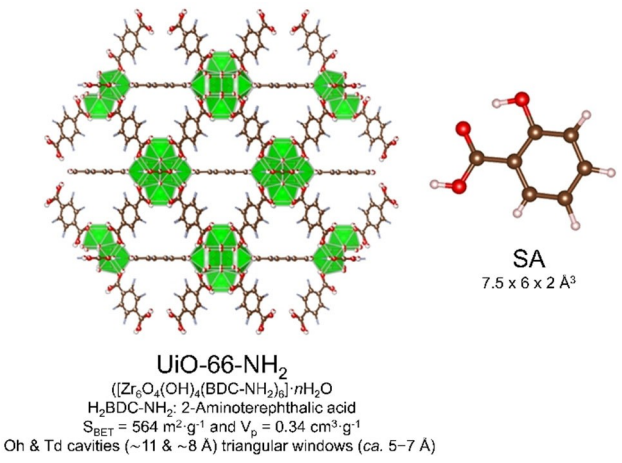

Figure 1. Schematic view of the structure of UiO-66-NH_2 (zirconium polyhedra, nitrogen, oxygen, and carbon atoms are represented in green, blue, red, and brown, respectively; the hydrogen atoms are omitted for clarity), its formula, and the description of its structure and porosity. SA chemical structure and its dimensions (size calculated from Vesta free software considering van der Waals radii) are also given.

First, SA encapsulation was studied in the selected porous MOFs by using two different MOF:SA molar ratios (1:2 and 1:0.5, **see Experimental Section for further details**-adsorption kinetics, fitting, and stability studies-, **Supporting Information S1**) to evaluate the influence of the drug concentration in the adsorption process. Although the SA incorporation was fast in all the studied MOFs, reaching a plateau after only 1 or 4 h, the amount of adsorbed SA strongly depends on the MOF and the **MOF:SA ratio** used. The amount of adsorbed SA (mg g^{-1}) in the tested materials follows similar order for each studied ratio, decreasing as follows: UiO-66-NH_2 > ZIF-8 > MIL-53 ≈ UiO-66 > MIL-53-$(OH)_2$ ≈ MIL-100 ≈ MIL-163 ≈ MIL-127 for MOF:SA ratio 1:0.5; and MIL-53 ≫ UiO-66-NH_2 ≫ MIL-53-$(OH)_2$ > UiO-66 > MIL-163 > ZIF-8 > MIL-100 ≈ MIL-127 for MOF:SA ratio 1:2. Although the SA (7.5×6×2 Å^3) is accessible to all the selected materials (see channels and windows sizes in Table 1), we can tentatively relate the SA adsorption capacity with the porosity of the framework (**pore size/windows dimensions**). Therefore, it is reasonable to suggest that high SA adsorption will be achieved in highly porous structures. However, the SA insertion experiments highlight a remarkable SA adsorption capacity in MOFs with a moderate porosity. For example, UiO-66-NH_2 shows a lower surface area than other studied MOFs (*e.g.*, lower that UiO-66), but a relatively high SA adsorption capacity (4-fold higher that UiO-66). Therefore, other factors may influence on SA capacity. In parallel, the **chemical and structural stability** of the MOFs during the SA adsorption experiment was tested by means of the leaching of the constitutive ligands by HPLC, and the crystallinity of the structure by PXRD, respectively. In SA aqueous solution, the chemical stability of the frameworks decreased in the following order: MIL-163 > MIL-53 ≈ UiO-66-NH_2 > MIL-127 > UiO-66 > MIL-100 > ZIF-8 ≈ MIL-53-$(OH)_2$ (Table 1). Further, PXRD patterns of the SA-containing MOFs evidenced that the SA loading process do not alter the crystallinity of the MOFs, except for the MIL-53 and MIL-53-$(OH)_2$, with a partial loss of crystallinity (Supporting Information,

Table 1. Pores and molecules dimensions (Å), Brunauer, Emmett and Teller surface areas (S_{BET}, $m^2 \cdot g^{-1}$), pore volume (V_p, $cm^3 \cdot g^{-1}$), MOF:SA ratio, adsorbed SA ($mol \cdot mol^{-1}$, and $mg \cdot g^{-1}$), and MOF degradation (%) for all studied materials.[a]

Structure	Pore or molecule size [Å]	Starting solid S_{BET} [$m^2 \cdot g^{-1}$] V_p [$cm^3 \cdot g^{-1}$]	Initial ratio (MOF:SA)	Adsorbed SA [$mol \cdot mol^{-1}$]	Adsorbed SA [$mg \cdot g^{-1}$]	MOF degradation [%]
SA	$7.5 \times 6 \times 2$ Å^3	–	–	–	–	–
UiO-66	Td (8 Å) & Oh (11 Å) cages accessible	1160	1:2	0.42	34.9	17.44 ± 0.13
	via triangular windows (5–7 Å)	0.50	1:0.5	0.15	12.8	20.57 ± 0.53
UiO-66-NH_2		950	1:2	1.54	121.42	5.49 ± 0.03
		0.34	1:0.5	0.75	59.0	4.07 ± 0.07
MIL-163	Square channels 12×12 Å^2	90–170[a]	1:2	0.06	17.9	0.00 ± 0.00
			1:0.5	0.01	3.6	0.00 ± 0.00
MIL-127	1D channels (6 Å) & cages (10 Å)	1300	1:2	0.01	1.7	4.17 ± 3.48
	accessible via 3 Å apertures	0.70	1:0.5	0.01	1.6	11.68 ± 4.58
MIL-53	7.5 Å (hydrated form)	–	1:2	0.63	367.9	0.78 ± 0.0
			1:0.5	0.03	14.5	6.30 ± 0.01
MIL-53-$(OH)_2$	9.1 Å (hydrated form)	–	1:2	0.14	71.8	41.94 ± 0.12
			1:0.5	0.01	7.4	26.88 ± 0.05
MIL-100	cages (25 & 29 Å)	1650	1:2	0.10	2.0	23.75 ± 0.35
	accessible via microporous windows (4.8–5.8 & 8.6 Å)	0.75	1:0.5	0.02	3.8	21.12 ± 0.37
ZIF-8	11.6 Å accessible through	1135	1:2	0.01	7.8	43.53 ± 0.10
	3.4 Å windows	0.54	1:0.5	0.03	20.5	23.68 ± 0.08

[a] Flexible matrix confirmed by a low N_2 adsorption compare to the expected from the structural analysis; Td, tetrahedral; Oh, octahedral.

Figure S2). This phenomenon could be related with the replacement of the carboxylate groups of the H_2BDC ligand by the carboxylic acid group of SA, leading to the framework degradation. This degradation is further confirmed by the appearance of a diffraction peak at $2\theta = 22.2°$, corresponding to the iron oxide formation,[36] ruling out the use of the MIL-53 series in the SA encapsulation and release.

Aside from the MOF:drug ratio, the porosity/accessibility and stability of the frameworks, other factors such as the **physico-chemical properties** of the MOFs (*e.g.*, hydrophobicity, polarity, electron polarizability, and size) might strongly influence on the SA loading.[37] First, SA is considered a lipophilic and hydrophobic molecule with a partition coefficient (log Pow) at room temperature of 2.26[38] and therefore, *a priori* it will be better adsorbed in hydrophobic matrices. Although MOFs possess both a polar part (metal clusters) and a more or less non-polar fraction (aromatic ligands), from all tested materials, ZIF-8 is the most hydrophobic material, UiO-66 and UiO-66-NH_2 show a moderate hydrophobicity, MIL-127 can be considered a hydrophilic/hydrophobic structure, and MIL-163, MIL-100, MIL-53 and MIL-53-$(OH)_2$ could be regarded as more hydrophilic materials.[39–41] These consideration fall mainly in the broad that low SA capacity is reached in hydrophilic MOFs while better total SA cargo is obtained in the hydrophobic ones. In a further step, and considering only the hydrophobic MOFs, UiO-66-NH_2 shows the highest SA loading rate when using both MOF:SA molar ratios.

This could be related with the presence of the amino functional group, as it can efficiently interact with SA by polarity matching and the potential formation of **hydrogen bonds** between the amino groups of the MOF and the phenolic hydroxyl and carboxyl groups of SA (see FTIR study in next section).[42]

Considering that UiO-66-NH_2 leads to the highest SA cargo (5.9 and 12.1 wt.% at MOF:SA 1:0.5 and 1:2 ratios, respectively), an impressive chemical and structural stability, and proper polarity, we selected this MOF for the subsequent cutaneous release of SA under simulated cutaneous conditions. In fact, SA content in the UiO-66-NH_2 is comparable or even higher than the one obtained with other materials currently used in the SA cutaneous delivery (*e.g.*, 2 wt.% in Carbopol®,[43] 5 wt.% cutaneous microdialysis,[44] 12 wt.% in chitosan-based nanoemulsion-films,[45] 15 wt.% in SA patches,[46] from 2 to 16.7 wt.% in 6 different topical formation,[47] 5–25 wt.% in self-emulsifiable formulation,[48] or 30 wt.% in polyethylene glycol).[49]

UiO-66-NH_2@SA: a detailed study

Considering the previous promising encapsulation results, we further characterized the SA loaded SA@UiO-66-NH_2 (with the maximum SA amount of 12.1 wt.%). As mentioned before, PXRD patterns evidence that the drug-loading process does not alter the crystalline structure of the UiO-66-NH_2 (Supporting Information, Figure S2). In addition, the absence of Bragg peaks corresponding to free SA rules out the presence of free recrystallized drug out of the pores. The drug content, estimated by HPLC, was confirmed by a combination of thermogravimetric analysis (TGA) and elemental analysis (EA, Supporting Information, Figure S3 and Table S2). The high SA loading (12.1 wt.%) corresponds to 1.54 mol of drug *per* mol of material. This value is in total agreement with the encapsulation rates obtained for pure UiO-66-NH_2 or its composites with other molecules (*i.e.*, 4.9 wt.% cisplatin,[50] and 27 wt.% 5-fluorouracil in UiO-66-NH_2;[51] or 8.7 wt.% of SA in Fe_3O_4@SiO_2@UiO-66-NH_2).[52] Notably, the incorporation of SA within the porosity of UiO-66-NH_2 was confirmed by the reduction of the N_2 sorption

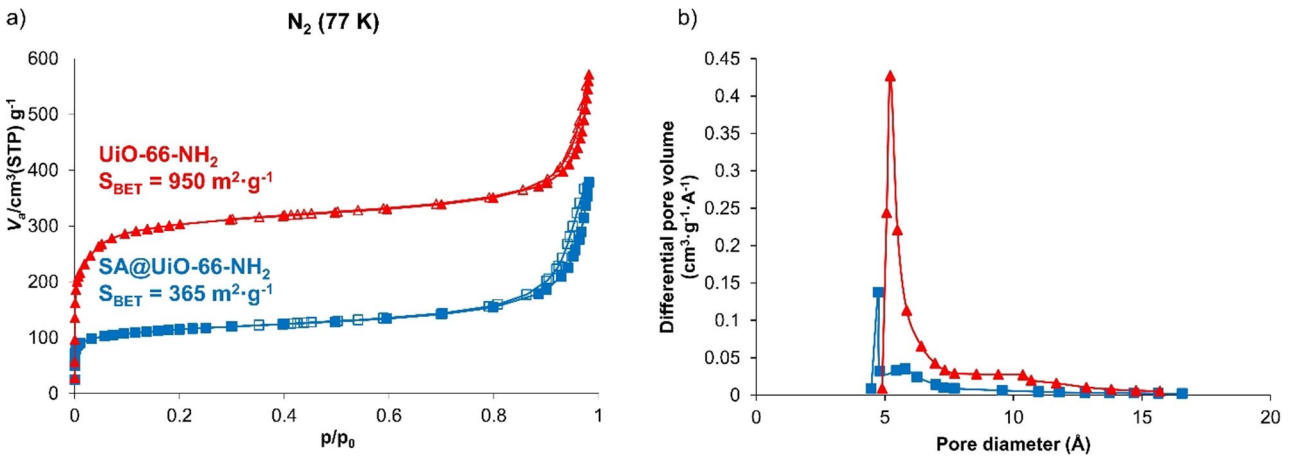

Figure 2. (a) N_2 sorption isotherms, and (b) pore distribution with Horvath-Kawazoe (KH) method of activated UiO-66-NH_2 (red) and SA@UiO-66-NH_2 (blue). Solid and empty symbols indicate adsorption and desorption branches, respectively.

capacity of the MOF (Figure 2; from the original UiO-66-NH_2 with $S_{BET} = 950\ m^2 \cdot g^{-1}$ and $V_p = 0.34\ cm^3 \cdot g^{-1}$, to the SA@UiO-66-$NH_2$ $S_{BET} = 365\ m^2 \cdot g^{-1}$, $V_p = 0.11\ cm^3 \cdot g^{-1}$) and the reduction of the pore size (Figure 2b). To shed some light on the influence of porosity on the drug adsorption, we estimated the volume occupied by one SA molecule inside the MOF by considering the variation of the MOF pore volume after the drug encapsulation ($\Delta V_p = 0.23\ cm^3 \cdot g^{-1}$) and the total amount of loaded drug ($1.54\ mol \cdot mol^{-1}$). The larger occupancy volume of SA in UiO-66-NH_2 (257 Å^3) compared to the free drug molecular volume (98 Å^3; estimated under vacuum) might be due to the partial occupancy of the porosity, as confirmed by the important remaining porosity after drug insertion. In this regard, one has to consider the correlation between size and shape of both the pores with the drug, determining whether the drug can be adsorbed. We note that the triangular windows of UiO-66-NH_2 (*ca.* 5–7 Å), giving access to both octahedral (Oh) and tetrahedral (Td) cavities (~11 and ~8 Å, respectively), seem to be large enough to allow the incorporation of the drug (7.5 × 6 × 2 Å^3) in both cages. Therefore, the non-perfectly efficient packing of the drug into the pores might lead to this important remaining porosity.

Finally, the FTIR spectroscopic analysis clearly shows the presence of the main bands of pure SA in the IR spectrum of SA@UiO-66-NH_2 (Supporting Information, Figure S4). The IR spectrum of SA@UiO-66-NH_2 confirmed a shift in the wavelengths in comparison with the bare UiO-66-NH_2 (from 3480 and 3367 cm^{-1} in the UiO-66-NH_2, to 3494 and 3380 cm^{-1} in the SA@UiO-66-NH_2, assigned to the $\nu_{as}(NH_2)$ and $\nu_s(NH_2)$ modes, respectively; and from 1334 and 1256 cm^{-1} in the UiO-66-NH_2, to 1338 and 1251 cm^{-1} in the SA@UiO-66-NH_2, assigned to the **ν**(C–N) modes). These shifts between samples may be indicative of the formation of specific interactions between the drug moieties and the UiO-66-NH_2 framework. One could tentatively propose the formation of hydrogen bonds between the carboxylic acid and hydroxyl groups in the SA with the NH_2 groups present within the MOF. This result seems to agree with the preferential adsorption of SA in the UiO-66-NH_2 when compared with its non-functionalized UiO-66 analogue.

Drug release

Once the SA@UiO-66-NH_2 was fully characterized, we evaluated its ability to deliver its active cargo to propose it as topical DDS. The delivery of the AS was performed in distilled water at 37 °C, under continuous bidimensional stirring, to assess a potential cutaneous administration, mimicking the skin hydration. The release kinetics was determined by quantifying the amount of delivered drug in the medium by HPLC as a function of time (Figure 3). According to the drug release profiles, the SA@UiO-66-NH_2 system shows a quite fast and partial SA release. A plateau in the SA release process from UiO-66-NH_2 is reached after 6 h (with a 64.3 ± 2.1 % or 105.6 mg of released SA *per* g of UiO-66-NH_2). After 24 h, the total amount of released drug is 66.8 % (or 103.3 mg of SA *per* g of UiO-66, Supporting

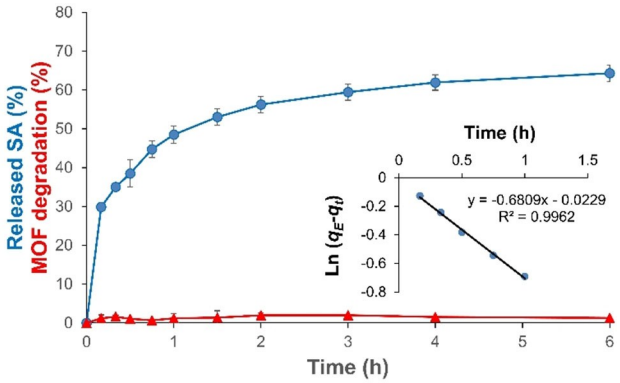

Figure 3. Released SA from UiO-66-NH_2 (blue) and MOF degradation (red) under simulated cutaneous conditions (aqueous media at 37 °C). The inset shows the fitting of the data to a first order kinetic model.

information, Figure S5). The release profile and the time to reach the plateau in play here is similar when further compared to previously delivery studies of SA in water (*e.g.*, 60% in 10 h from halloysite nanotubes;[53] 50% in 15 min from the microporous zeolite NaY, and the mesoporous SBA-15 and MCM-41).[54]

The desorption data can be satisfactorily fitted to a first order kinetic model according to Equation (1):

$$q_E - q_t = q_E \cdot e^{-kt} \quad (1)$$

where q_E and q_t are the amounts of released SA *per* gram of MOF ($mmol \cdot g^{-1}$) at the equilibrium and at the time *t*(h), respectively, and *k* is the first order kinetic constant. In a typical first order kinetics, the drug release rate exclusively depends on its concentration. The fitting of the data gives rise to a *k* value of 0.68 h^{-1} which correspond to a $t_{1/2}$ for the release of SA of 1 h (Figure 3). This is indicative of the SA physisorption on UiO-66-NH_2, ruling out its chemical binding. To confirm the stability of the MOF matrix, the leaching of the ligand to the water medium was further monitored by HPLC, confirming the stability of the MOF (*ca.* 2% of degradation after 4 days).

Taking into account that optimal cutaneous systems are usually applied for a maximum of 8–24 h period,[55] the structural stability of the obtained matrix after the SA delivery (denoted as SA@UiO-66-NH_2_del), and the evaluation of the residual amount of SA were studied by XRPD, FTIR, TGA and sorption measurements. FEG-SEM images denoted no significant morphological changes among all the studied samples (Figure S7).

The presence of the main bands of pure SA in the IR spectrum of UiO-66-NH_2@SA_del suggests the partial release of the drug (Supporting Information, Figure S6). These results agree with the TGA, exhibiting a residue between the SA loaded and the empty starting materials (40.3%, corresponding to the release of the 72% of SA). The structural integrity of the obtained SA@UiO-66-NH_2_del in water after 3 days monitored by PXRD indicates that the crystallinity is kept. This agrees with the very low ligand leaching in water media, as estimated by HPLC (*ca.* 2%). Therefore, one can conclude that UiO-66-NH_2 remains stable during the whole delivery process, making this safe material an excellent candidate for its use as cutaneous DDS.

Conclusion

The encapsulation of SA in MOFs is a promising alternative to overcome its topical administration, hindered by its reactivity/instability. Particularly, UiO-66-NH_2 combines an important SA cargo (12.1 wt.%) and an exceptional stability, with a release kinetics adapted to the cutaneous route (64% in 6 h), fulfilling the requirements of a topical DDS.

Experimental Section

All reactants were commercially obtained and used without further purification. The 5,5′-(1,2,4,5-tetrazine-3,6-diyl)bis(benzene-1,2,3-triol) ligand (H_6TzGal),[30] and the 3,3′,5,5′-azobenzenetetracarboxylic acid ligand (H_4TazBz)[56] were prepared as previously described in literature. Triethyl-1,3,5-benzenetricarboxylate (Et_3BTC) was prepared by heating under reflux 24 mmol (5 g) of trimesic acid (H_3BTC) in a solution of 2 mL of H_2SO_4 in 100 mL of ethanol absolute and for 24 h. The obtained Et_3BTC was filtered and washed with water.

Synthesis of MOFs

The synthesis of starting MOFs was performed following similar procedures previously reported.

UiO-66 and **UiO-66-NH_2** or $[Zr_6O_4(OH)(C_8H_3O_4X)_6]$ nH_2O, X = H or NH_2.[29,57] 1 mmol (233.03 mg) of $ZrCl_4$ and 1 mmol of dicarboxylic linker (terephthalic acid - H_2BDC, 166.13 mg; or 2-aminoterephthalic acid – H_2BDC-NH_2, 181.15 mg) were dispersed in 3 mL of *N*,*N*-dimethylformamide (DMF), placed in a teflon-lined autoclave and heated for 12 h at 220 °C (UiO-66) or 24 h at 100 °C (UiO-66-NH_2). The resulting solid was recovered by filtration and washed with deionized water and acetone. 200 mg of the solid were suspended in 100 mL of DMF under stirring for 12 h. Then, the DMF-washed solid was suspended in 100 mL of methanol (MeOH) under stirring for 12 h, recovering the activated solid by filtration. UiO-66 and UiO-66-NH_2 samples were evacuated for 12 h at 200 and 150 °C, respectively.

MIL-163 or $[Zr_2(C_{14}H_2O_6N_4)_2]\cdot(DMA)_5(H_2O)_{14}$, DMA: *N*,*N*-dimethylamine.[30] In a 25 mL teflon-lined steel autoclave, 0.2 mmol (47 mg) of $ZrCl_4$ was added to a solution of 0.4 mmol of the 5,5′-(1,2,4,5-tetrazine-3,6-diyl)bis(benzene-1,2,3-triol) ligand (H_6TzGal, 132 mg) in DMA (2 mL) at RT. Deionized water (3 mL) was then added under stirring, and the autoclave sealed and placed in the oven for 24 h at 130 °C. After cooling to RT, the solution was filtered and MIL-163 was recovered as a dark-red fine powder. The solid was then washed in DMF (10 mL) and ethanol (EtOH, 10 mL) for one night with each, before being filtered and dried in air.

MIL-127 or $[Fe_3O(OH)_{0.88}Cl_{0.12}(C_{16}N_2O_8H_6)_{1.5}(H_2O)_3]\cdot nH_2O$.[32] The solution obtained by adding 0.927 g of NaOH to 26 mL of propan-2-ol in a 250 mL round-bottom flask, was stirred until complete dissolution of NaOH. After the addition of 10.1 mmol (3.636 g) of 3,3′,5,5′-azobenzenetetracarboxylic acid ligand (H_4TazBz), the resulting solution was stirred at 90 °C. In parallel, 20 mmol (5.498 g) of $FeCl_3\cdot 6H_2O$ were dissolved in 14 mL of propan-2-ol in a flask at 70 °C. In the next step, a mixture obtained by mixing the iron and the ligand solutions was stirred under reflux for 24 h. A crystalline powder was recovered by filtration, washed with 200 mL of distilled water, 200 mL of propan-2-ol, and finally with 200 mL of ethanol. MIL-127 was evacuated for 12 h at 150 °C.

MIL-53 or $[Fe(OH)(C_8O_4H_4)]\cdot nH_2O$.[3] 0.1 mol (27 g) of $FeCl_3.6H_2O$ and 0.1 mol (16.6 g) of H_2BDC were dispersed in 500 mL of DMF. The mixture was placed in a round bottom flask and refluxed for 48 h at 150 °C under stirring. Then, the yellow solid was recovered by filtration and washed with DMF. Then, the solid was suspended in 500 mL of water for 12 h. MIL-53 was evacuated for 12 h at 200 °C.

MIL-53-$(OH)_2$ or $[Fe(OH)(C_8H_4O_6)]$.[34] 6.8 mmol (1.34 g) of 2,5-dihydroxyterephthalic acid (H_2BDC-$(OH)_2$), 4.6 mmol (1.63 g) of $Fe(ClO_4)_3\cdot H_2O$, 25 mL of DMF, 1 mL of a 5 M hydrofluoric acid solution and 5 mL of a 5 M perchloric acid solution were placed in a 125 mL teflon-lined steel autoclave. The mixture stirred for 10 minutes, the autoclave sealed, and placed in an oven at 100 °C for

16 h. Crude MIL-53-$(OH)_2$ was recovered as a dark crystalline solid by filtration, washed with ethanol and dried in air. MIL-53-$(OH)_2$ sample was evacuated for 12 h at 130 °C.

MIL-100 or $[Fe_3O(H_2O)_2OH(C_6H_3(CO_2)_3)_2]$ nH_2O. First, triethyl-1,3,5-benzenetricarboxylate (Et_3BTC) was prepared by heating under reflux 24 mmol (5 g) of H_3BTC in a solution of 2 mL of H_2SO_4 in 100 mL of ethanol absolute and for 24 h. The obtained Et_3BTC was filtered and washed with water. MIL-100 was prepared from hydrothermal reaction (125 mL vessel) of 10 mmol (2.7 g) of $FeCl_3$ $6H_2O$ and 6.6 mmol (1.94 g) of Et_3BTC in 50 mL of water for 3 days at 130 °C.

ZIF-8 or $[Zn(C_4H_5N_2)_2]$ nH_2O.[35] 2.5 mmol (0.744 g) of $Zn(NO_3)_2 \cdot 6H_2O$ was dissolved in 10 mL of deionized water and added to a solution of 0.21 mmol of 2-methylimidazole (Hmim, 0.172 g) in 90 mL of deionized water. The mixture was stirred at room temperature. The solution quickly became cloudy and a suspension was obtained. 24-hours later, the suspension was centrifuged and washed with methanol three times. The products were then dried for 24 h under reduced pressure at 40 °C.

Analysis and Characterization

Physicochemical characterization. Fourier transform infrared (FTIR) spectroscopic analyses were performed in a Thermo Scientific Nicolet 6700. KBr pellets of the UiO-66-NH_2 and SA@UiO-66-NH_2 were prepared and dried overnight at 100 °C before the measurement. N_2 isotherms were obtained at 77 K using Belsorp Max (Bel, Japan). Before the measurements, UiO-66-NH_2 and SA@UiO-66-NH_2 were evacuated at 150 °C for 12 h (see evacuation process for the rest of MOFs in the **Synthesis of MOF section**). Specific surface area was determined by applying Brunauer, Emmett & Teller equation (BET) in the relative pressure interval $p/p_0 = 0.01–0.3$ (being p_0 the saturation pressure). Pore volume (V_p) and pore size distribution were calculated by the non-localized density functional theory (NLDFT) and the Horvath-Kawazoe (KH) methods, respectively. Routine X-ray powder diffraction (PXRD) patterns were collected using a conventional high resolution D5000 Siemens X'Pert MDP diffractometer (θ–2θ) using λ_{Cu} $K_{\alpha1}$, and $K_{\alpha2}$ radiation ($\lambda = 1.54051$ and 1.54433 Å), from 3 to 35 or 60 (2θ), a step size of 0.02°, and 2 s·step^{-1} in continuous mode, and a conventional PANalytical Empyrean powder diffractometer (PANalytical Lelyweg, Netherlands, θ–2θ) using the same λ_{Cu} $K_{\alpha1}$, and $K_{\alpha2}$ radiation. Thermogravimetric analyses (TGA) were performed using a Perkin-Elmer Diamond TGA/DTA STA 6000 running form room temperature (RT) to 600 °C with a heating rate of 2 °C·min^{-1}. Field emission gun-scanning electron microscopy (FEG-SEM) images were acquired in a FEI/Philips XL-30 Field Emission ESEM (Philips, Amsterdam, The Netherlands) at 3 kV and 98–102 μA.

High performance liquid chromatography (HPLC). The amount of adsorbed SA, as well as the potential release of the corresponding organic linker, were determined using a reversed phase HPLC Jasco LC-4000 series system, equipped with a PDA detector MD-4015 and a multisampler AS-4150 controlled by ChromNav software (Jasco Inc, Japan). A Purple ODS reverse phase column (5 μm, 4.6× 150 mm, Análisis Vínicos, Spain) was employed. For the quantification of all chemical species, isocratic conditions were used. The flow rate was 1 mL·min^{-1}, and the column temperature was fixed at 298 K. In all cases, the injection volume was 30 μL. The mobile phase was based on a mixture of 50:50 MeOH:phosphate buffered solution (PBS; 0.04 M, pH = 2.5) for SA and MOFs' ligand analysis was used with different retention time (rt) and absorption maximum (λ) for each molecule: SA (rt = 4.99 min, λ = 231 nm), H_2BDC (rt = 3.98 min, λ = 240 nm), H_2BDC-NH_2 (rt = 3.03 min, λ = 228 nm), H_2BDC-$(OH)_2$ (rt = 2.92 min, λ = 217 nm), 3,3',5,5'-azobenzenetetracarboxylic acid (H_4TazBz, rt = 16.36 min, λ = 311 nm), H_3BTC (rt = 3.51 min, λ = 225 nm), Hmim (rt = 1.8 min, λ = 205 nm), and 5,5'-(1,2,4,5-tetrazine-3,6-diyl)bis(benzene-1,2,3-triol) (H_6TzGal, rt = 3.24 min, λ = 360 nm).

Preparation of the phosphate buffered solution (0.04 M, pH = 2.5): 0.02 mol (2.4 g) of NaH_2PO_4 and 0.02 mol (2.84 g) of Na_2HPO_4 were dissolved in 1 L of Milli-Q water. The pH was then adjusted to 2.5 with H_3PO_4 (≥ 85 %).

Adsorption and stability studies. SA adsorption studies were performed by suspending 30 mg of desolvated MOFs in 30 mL of deionized water containing different amount of SA. The MOF:SA molar ratios were 1:2 and 1:0.5, using SA concentration from 44.8 to 1369.8 mg·L^{-1}. The suspensions were stirred under bidimensional continuous stirring (80×80 rpm) at 25 °C for 24 h. At different incubation times, the suspensions were centrifuged (14500 rpm, 10 min), and filtered with a syringe filter (0.2 μm) to obtain clean solutions. The obtained solids were characterized by PXRD to check their crystallinity, while the liquid phases were analyzed by HPLC, determining the amount of SA and the total amount of possible MOF's leached ligand in the solution. All the SA studies and leached ligand determinations were performed by triplicate. *Drug release.* 10 mg of the drug-containing MOF (SA@UiO-66-NH_2) was placed in 10 mL of deionized water at 37 °C under bidimensional continuous stirring (80×80 rpm). At different incubation times, 5 mL of supernatant was recovered by centrifugation (13000 rpm for 10 min) and replaced with the same volume of fresh deionized water at 37 °C. This procedure was performed in triplicate. The amount of released drug and the possible leached ligand were determined by HPLC. After the drug-delivery process, the sample was characterized by PXRD, FTIR spectroscopy, and TGA.

Acknowledgements

S.R. and P.H. acknowledge the regional Madrid founding (Talento 2017 Modality 2, 2017-T2/IND-5149), MOFSEIDON project (PID2019-104228RB-I00, MCI/AEI/FEDER, UE), and the Multifunctional Metallodrugs in Diagnosis and Therapy Network (MICIU, RED2018-102471-T). P.H. thanks the Spanish Ramón y Cajal Programme (grant agreement 2014-16823). S. R. thanks the Juan de la Cierva Incorporación Fellowship (grant agreement IJC2019-038894-I).

Conflict of Interest

The authors declare no conflict of interest.

Keywords: Metal-organic frameworks · Drug delivery · Salicylic acid · Cutaneous treatment · Water stability

[1] V. P. Torchilin, *Nanoparticulates as Drug Carriers*, London, **2006**.
[2] M. Giménez-Marqués, T. Hidalgo, C. Serre, P. Horcajada, *Coord. Chem. Rev.* **2015**, *307*, 342–360.
[3] P. Horcajada, T. Chalati, C. Serre, B. Gillet, C. Sebrie, T. Baati, J. F. Eubank, D. Heurtaux, P. Clayette, C. Kreuz, J.-S. Chang, Y. K. Hwang, V. Marsaud, P.-N. Bories, L. Cynober, S. Gil, G. Férey, P. Couvreur, R. Gref, *Nat. Mater.* **2010**, *9*, 172–178.
[4] P. Horcajada, R. Gref, T. Baati, P. K. Allan, G. Maurin, P. Couvreur, G. Férey, R. E. Morris, C. Serre, *Chem. Rev.* **2012**, *112*, 1232–1268.
[5] H. C. J. Zhou, S. Kitagawa, *Chem. Soc. Rev.* **2014**, *43*, 5415–5418.

[6] C. Doonan, R. Riccò, K. Liang, D. Bradshaw, P. Falcaro, *Acc. Chem. Res.* **2017**, *50*, 1423–1432.
[7] C. Orellana-Tavra, R. J. Marshall, E. F. Baxter, I. A. Lázaro, A. Tao, A. K. Cheetham, R. S. Forgan, D. Fairen-Jimenez, *J. Mater. Chem. B* **2016**, 7697–7707.
[8] P. Horcajada, C. Serre, M. Vallet-Regí, M. Sebban, F. Taulelle, G. Férey, *Angew. Chem. Int. Ed.* **2006**, *45*, 5974–5978; *Angew. Chem.* **2006**, *118*, 6120–6124.
[9] A. G. Márquez, T. Hidalgo, H. Lana, D. Cunha, M. J. Blanco-Prieto, C. Álvarez-Lorenzo, C. Boissière, C. Sánchez, C. Serre, P. Horcajada, *J. Mater. Chem. B* **2016**, *4*, 7031–7040.
[10] S. Rojas, P. S. Wheatley, E. Quartapelle-Procopio, B. Gil, B. Marszalek, R. E. Morris, E. Barea, *CrystEngComm* **2013**, *15*, 9364–9367.
[11] A. C. Mckinlay, J. F. Eubank, S. Wuttke, B. Xiao, P. S. Wheatley, P. Bazin, M. Daturi, A. Vimont, G. De Weireld, P. Horcajada, C. Serre, R. E. Morris, *Chem. Mater.* **2013**, *88*, 1592–1599.
[12] F. J. Carmona, S. Rojas, C. C. Romão, J. A. R. Navarro, E. Barea, C. R. Maldonado, *Chem. Commun.* **2017**, *53*, 6581–6584.
[13] Markets&Markets, *Topical Drug Delivery Market*, **2020**.
[14] N. Kanikkannan, S. Kandimalla, S. S. Lamba, M. Singh, *Curr. Med. Chem.* **2000**, *7*, 593–608.
[15] J. R. Vane, R. M. Botting, *Am. J. Med.* **1998**, *104*, 2S–8S.
[16] J. R. Paterson, J. R. Lawrence, *QJM – Mon. J. Assoc. Physicians* **2001**, *94*, 445–448.
[17] C. L. Campbell, *Jama* **2007**, *297*, 1–7.
[18] R. Amann, B. A. Peskar, *Eur. J. Pharmacol.* **2002**, *447*, 1–9.
[19] S. D. Taherzade, S. Rojas, J. Soleimannejad, P. Horcajada, *Nanomaterials* **2020**, *10*, 2296–2316.
[20] S. Rojas, T. Baati, L. Njim, L. Manchego, F. Neffati, N. Abdejelil, S. Saguem, C. Serre, M. F. M. F. Najjar, A. Zakhama, P. Horcajada, N. Abdeljelil, S. Saguem, C. Serre, M. F. M. F. Najjar, A. Zakhama, P. Horcajada, *J. Am. Chem. Soc.* **2018**, *140*, 9581–9586.
[21] S. Rojas, N. Guillou, P. Horcajada, *ACS Appl. Mater. Interfaces* **2019**, *11*, 22188–22193.
[22] "http://jp-minerals.org/vesta/en/," **2020**.
[23] T. Baati, L. Njim, F. Neffati, A. Kerkeni, M. Bouttemi, R. Gref, M. F. Najjar, A. Zakhama, P. Couvreur, C. Serre, P. Horcajada, *Chem. Sci.* **2013**, *4*, 1597–1607.
[24] À. Ruyra, A. Yazdi, J. Espín, A. Carné-Sánchez, N. Roher, J. Lorenzo, I. Imaz, D. Maspoch, *Chem. A Eur. J.* **2015**, *21*, 2508–2518.
[25] A. Ruyra, A. Yazdi, J. Espín, A. Carné-Sánchez, N. Roher, J. Lorenzo, I. Imaz, D. Maspoch, *Chem. A Eur. J.* **2015**, *21*, 2508–2518.
[26] M. Hoop, C. F. Walde, R. Riccò, F. Mushtaq, A. Terzopoulou, X. Z. Chen, A. J. de Mello, C. J. Doonan, P. Falcaro, B. J. Nelson, J. Puigmartí-Luis, S. Pané, *Appl. Mater. Res.* **2018**, *11*, 13–21.
[27] G. Chen, X. Leng, J. Luo, L. You, C. Qu, X. Dong, H. Huang, X. Yin, J. Ni, *Molecules* **2019**, *24*, DOI 10.3390/molecules24071211.
[28] P. Ghosh, Y. J. Colón, R. Q. Snurr, *Chem. Commun.* **2014**, *50*, 11329–11331.
[29] J. H. Cavka, S. Jakobsen, U. Olsbye, N. Guillou, C. Lamberti, S. Bordiga, K. P. Lillerud, *J. Am. Chem. Soc.* **2008**, *130*, 13850–13851.
[30] G. Mouchaham, L. Cooper, N. Guillou, C. Martineau, E. Elkaïm, S. Bourrelly, P. L. Llewellyn, C. Allain, G. Clavier, C. Serre, T. Devic, *Angew. Chem. Int. Ed. Engl.* **2015**, *54*, 13297–13301.
[31] Y. Liu, J. F. Eubank, A. J. Cairns, J. Eckert, V. C. Kravtsov, R. Luebke, M. Eddaoudi, *Angew. Chem. Int. Ed. Engl.* **2007**, *46*, 3278–3283.
[32] H. Chevreau, A. Permyakova, F. Nouar, P. Fabry, C. Livage, F. Ragon, A. Garcia-Marquez, T. Devic, N. Steunou, C. Serre, P. Horcajada, *CrystEngComm* **2016**, *18*, 4094–4101.
[33] P. Horcajada, S. Surblé, C. Serre, D.-Y. Hong, Y.-K. Seo, J.-S. Chang, J.-M. Grenèche, I. Margiolaki, G. Férey, *Chem. Commun.* **2007**, *100*, 2820–2822.
[34] T. Devic, P. Horcajada, C. Serre, F. Salles, G. Maurin, D. Heurtaux, G. Clet, A. Vimont, J. Grene, B. Le Ouay, F. Moreau, E. Magnier, Y. Filinchuk, J. Lavalley, M. Daturi, I. Charles, G. Montpellier, *J. Am. Chem. Soc.* **2010**, *132*, 1127–1136.
[35] V. A. Online, K. Kida, M. Okita, K. Fujita, S. Tanaka, Y. Miyake, *CrystEngComm* **2013**, *15*, 1794–1801.
[36] E. Ghasemi, A. Mirhabibi, M. Edrissi, R. Aghababazadeh, R. M. Brydson, *J. Nanosci. Nanotechnol.* **2009**, *9*, 4273–4278.
[37] S. Rojas, I. Colinet, D. Cunha, T. Hidalgo, F. Salles, C. Serre, N. Guillou, P. Horcajada, *ACS Omega* **2018**, *3*, 2994–3003.
[38] C. Hansch, A. Leo, D. Hoekman, *J. Med. Chem.* **1996**, *39*, 1189–1190.
[39] L. H. Xie, M. M. Xu, X. M. Liu, M. J. Zhao, J. R. Li, *Adv. Sci.* **2020**, *7*, 1901758–1901802.
[40] P. G. M. Mileo, Computational Exploration of Water Adsorption and Proton Conduction in Porous Materials, Université Montpellier, **2019**.
[41] J. Canivet, A. Fateeva, Y. Guo, B. Coasne, D. Farrusseng, *Chem. Soc. Rev.* **2014**, *43*, 5594–5617.
[42] J. Huang, X. Jin, J. Mao, B. Yuan, R. Deng, S. Deng, *J. Hazard. Mater.* **2012**, *217–218*, 406–415.
[43] "Anti-Acne Treatment Cream with 2% Salicylic Acid (Formulation #O-0057)," can be found under https://www.ulprospector.com/es/eu/PersonalCare/Detail/77/238019/Anti-Acne-Treatment-Cream-with-2-Salicylic-Acid-Formulation-O-0057, **2020**.
[44] A. Klimowicz, S. Farfał, S. Bielecka-Grzela, *J. Clin. Pharm. Ther.* **2007**, *32*, 143–148.
[45] T. N. da Silva, F. Reynaud, P. H. de S. Picciani, K. G. de Holanda, E. Silva, T. N. Barradas, *Int. J. Biol. Macromol.* **2020**, *164*, 2558–2568.
[46] J. H. Mottaz, P. J. Mckeever, J. L. Neveaux, A. S. Zelickson, *Int. J. Dermatol.* **1988**, *27*, 596–600.
[47] J. C. Tsai, S. A. Chuang, M. Y. Hsu, H. M. Sheu, *Int. J. Pharm.* **1999**, *188*, 145–153.
[48] B. C. Sekhar, *Topical Composition for Delivery of Salicylates*, **2007**.
[49] S. Ueda, K. Mitsugi, K. Ichige, K. Yoshida, T. Sakuma, S. I. Ninomiya, T. Sudou, *J. Dermatol. Sci.* **2002**, *28*, 211–218.
[50] K. A. Mocniak, I. Kubajewska, D. E. M. Spillane, G. R. Williams, R. E. Morris, *RSC Adv.* **2015**, *5*, 83648–83656.
[51] S. Tai, W. Zhang, J. Zhang, G. Luo, Y. Jia, M. Deng, Y. Ling, *Microporous Mesoporous Mater.* **2016**, *220*, 148–154.
[52] R. Zhang, Z. Wang, Z. Zhou, D. Li, T. Wang, P. Su, Y. Yang, *Ind. Eng. Chem. Res.* **2019**, *58*, 3876–3884.
[53] L. Ghezzi, A. Spepi, M. Agnolucci, C. Cristani, M. Giovannetti, M. R. Tiné, C. Duce, *Appl. Clay Sci.* **2018**, *160*, 88–94.
[54] N. Vilaça, F. Morais-Santos, A. F. Machado, A. Sirkecioğlu, M. F. R. Pereira, M. Sardo, J. Rocha, P. Parpot, A. M. Fonseca, F. Baltazar, I. C. Neves, *J. Phys. Chem. C* **2015**, *119*, 3589–3595.
[55] K. S. Paudel, M. Milewski, C. L. Swadley, N. K. Brogden, P. Ghosh, A. L. Stinchcomb, *Ther. Delivery* **2010**, *1*, 109–131.
[56] A. Dhakshinamoorthy, M. Alvaro, H. Chevreau, P. Horcajada, T. Devic, H. Garcia, *Catal. Sci. Technol.* **2012**, *3*, 324–330.
[57] M. Kandiah, M. H. Nilsen, S. Usseglio, S. Jakobsen, U. Olsbye, M. Tilset, C. Larabi, E. A. Quadrelli, F. Bonino, K. P. Lillerud, D. Lyon, *Chem. Mater.* **2010**, *10*, 6632–6640.

Manuscript received: December 18, 2020
Revised manuscript received: February 25, 2021
Accepted manuscript online: March 1, 2021